Research Article | Vol. 9, No. 6 / 1 June 2019 / Optical Materials Express 2573

Optical Materials EXPRESS

Photonic micro-structures produced by selective etching of laser-crystallized amorphous silicon

G. Martinez-Jimenez,[1] Y. Franz,[1] A. F. J. Runge,[1,2] M. Ceschia,[1] N. Healy,[3] S. Z. Oo,[1,4] A. Tarazona,[1] H. M. H. Chong,[4] A. C. Peacock,[1] and S. Mailis[1,5,*]

[1]Optoelectronics Research Centre, University of Southampton, Highfield, Southampton, SO17 1BJ, UK
[2]Current address: Institute of Photonics and Optical Science (IPOS), School of Physics, University of Sydney, NSW, Australia
[3]Emerging Technology and Materials Group, Newcastle University, Merz Court, Newcastle, NE1 7RU, UK
[4]School of Electronics and Computer Science, University of Southampton, Highfield, Southampton, SO17 1BJ, UK
[5]Current address: Skolkovo Institute of Science and Technology, Novaya St. 100, Skolkovo 143025, Russia
*s.mailis@skoltech.ru

Abstract: We present a method for the production of polycrystalline Si (poly-Si) photonic micro-structures based on laser writing. The method consists of local laser-induced crystallization of amorphous silicon (a-Si) followed by selective etching in chemical agents that act preferentially on the a-Si material, consequently revealing the poly-Si content of the film. We have studied the characteristics of these structures as a function of the laser processing parameters and we demonstrate their potential photonic functionality by fabricating polycrystalline silicon ridge optical waveguides. Preliminary waveguide transmission performance results indicated an optical transmission loss of 9 dB/cm in these unrefined devices.

1. Introduction

Silicon (Si) is a material that is synonymous to microelectronics, yet for several years it has been penetrating the area of photonics and today it forms an important sector of integrated optics. The mature processing technology of Si, which is available in foundries around the world is also applicable to the manufacturing of photonic devices and so many important innovations have been achieved in this rapidly evolving area of technology [1,2]. The bulk of silicon photonics research involves single crystal material, however polycrystalline silicon (poly-Si) has attracted significant interest because of its potential to combine good optical transmission (in the telecom and near IR wavelength range), electronic functionality and low fabrication cost, which makes it an attractive material for commercial applications[3,4]. Poly-Si films can be grown using various techniques. However, the utility of the resulting material is a function of the crystalline grain size, therefore high temperature growth is required [4–6]. Another possibility is the low temperature deposition of a-Si followed by post crystallization using methods such as laser irradiation. It has been shown recently that laser processing of amorphous silicon (a-Si) produces poly-Si with very large domain sizes, resulting in a material with superior optical and electronic performance [7].

C.W. laser-induced crystallization of a-Si on SiO_2 has been demonstrated in the literature [8,9] and has been shown to produce crystal domains with very high aspect ratio. Interestingly, laser-induced crystallization of silicon in a confined volume results in significant strain due to the difference in volume between the amorphous and crystalline states of the material, which in turn

#363769 https://doi.org/10.1364/OME.9.002573
Journal © 2019 Received 1 Apr 2019; accepted 17 Apr 2019; published 14 May 2019

Optical Materials EXPRESS

results in large shifts of the bandgap energy of the crystallized material as compared to regular silicon [9].

In a recent report a laser writing method has been proposed for the production of low loss poly-Si waveguides by laser-induced crystallization of photolithographically pre-defined a-Si ridge structures [7]. The localised nature of this method as well as the low temperature hot-wire chemical vapour deposition (HWCVD) [10,11] that was used to produce the initial a-Si film makes this method suitable for additive manufacturing, in contrast to previous reports, that required high temperature grown poly-Si [4–6]. Here we demonstrate a method where spatially selective laser-induced crystallization of a-Si produces poly-Si super structures with photonic functionality that does not require any pre-structuring step. Selective laser irradiation of planar a-Si films produces areas of poly-Si into the original a-Si film matrix. These areas transform into superstructures after subjecting the film to etching agents, which remove preferentially the a-Si content of the film, thus revealing the poly-Si structure. Such poly-Si ridges can be used as optical waveguides to transmit light. A schematic representation of the processing steps is shown in Fig. 1.

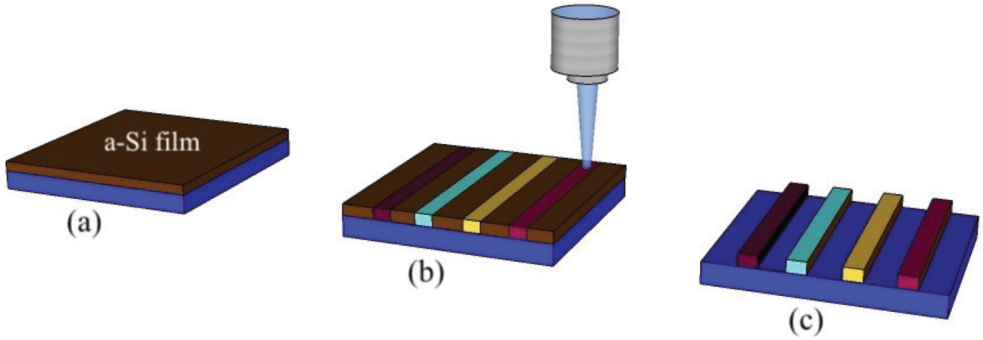

Fig. 1. Schematic of the process showing (a) a-Si film deposition by HWCVD on a planar substrate (b) spatially selective laser exposure by scanning of a focussed beam on the surface of the film to produce poly-Si tracks and (c) poly-Si tracks transform into ridge structures after selective etching. Different coloured tracks represent different irradiation conditions.

2. Experiments and discussion

2.1. Laser irradiation

Laser irradiation experiments were performed on a-Si films that were prepared by low temperature (320°C) HWCVD. The deposition conditions were adjusted to minimise the hydrogen content of the deposited material, to avoid violent hydrogen out-gassing during the irradiation step. Films of a-Si with two different thicknesses 210 nm and 425 nm) were deposited onto fused silica (SiO_2) and silica-on silicon substrates. The latter consists of a ~4.8 μm thick thermally oxidised top layer of bulk single crystal Si .

The films were subsequently exposed to a focussed laser beam using a set of a high precision translation stages (Aerotech, ABL1500), which offered excellent positioning control with constant, adjustable speed, thus maintaining identical exposure conditions along each irradiated track. The laser radiation source was a C.W. Ar^+ laser operating in multi wavelength mode (predominantly λ=488/514.5 nm). Linear tracks were irradiated using a range of beam intensities, scanning speeds, and beam spot sizes, which are the processing parameters available. The laser intensity, which can be adjusted by changing the laser power and/or the laser spot size, defines the peak temperature of the irradiated volume. The scanning speed controls the dwell time of the laser

Optical Materials EXPRESS

beam at a particular area on the sample, which defines the duration of the heating and influences the cooling rate of the laser-heated volume.

The laser intensities that are required for laser-induced crystallization can only be accessed by focussing the beam of the laser that was used. In these experiments we used three different microscope objectives: ×10 (NA=0.25), ×20 (NA=0.40), and ×40 (NA=0.65) producing laser spot sizes (beam radius at $1/e^2$ intensity level) of: 3 μm, 1.2 μm and 0.9 μm respectively, as measured using a knife-edge method.

It has been shown in [9] that temperatures as high as the melting point for a-Si can be achieved as a result of laser irradiation. This is due to the very efficient absorption of visible radiation by a-Si (absorption length ~ 30nm). Localised melting and re-solidification produce changes to the texture of the surface as well as a volume change in the transition from a-Si to poly-Si [9]. Both effects contribute into making the tracks visible under optical microscopy investigation. Figure 2 shows optical microscopy images of laser-irradiated tracks on an 400 nm thick a-Si film, deposited on SiO_2. This particular set consists of 7 track pairs, with the tracks in each pair irradiated with the same laser intensity using a laser spot size spot size of 3 μm. The irradiating laser intensity increased from right to left within the range of $5x10^5$W/cm^2- $9x10^5$ W/cm^2. The difference in colour of the material on the track is indicative of changes in the film thickness and/or refractive index, with the tracks becoming wider with increasing laser intensity. For scans at the high end of the laser intensity, structural damage can be observed along the centreline of the tracks.

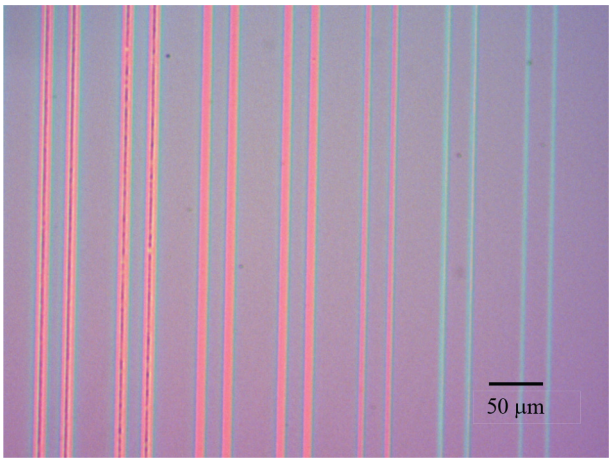

Fig. 2. Optical microscopy image of laser irradiated tracks on a planar a-Si film. The tracks are arranged in pairs of identical laser irradiation confitions. The laser intensity increases from right to left.

2.2. Raman spectroscopy

Figure 3 shows Raman spectra that were acquired from a laser irradiated track and from the non-irradiated surrounding film area illustrating the transformation of the original amorphous material, which produces a broad Raman response (blue line), to crystalline that produces a sharp, narrow Raman resonance located close to 520 cm^{-1} (orange line), where the single crystal Si Raman peak appears, indicating that crystalline Si is produced as a result of laser irradiation.

The width and position of the Raman peaks provide information about the a-Si/c-Si ratio and any stress that is locked in the crystallized material [7,12]. The Raman peaks, obtained from the laser-irradiated tracks were fit with a Voigt function [13]. Performing a Voigt curve fitting on the Raman peak obtained from a single crystal sample, used as reference, and by

Optical Materials EXPRESS

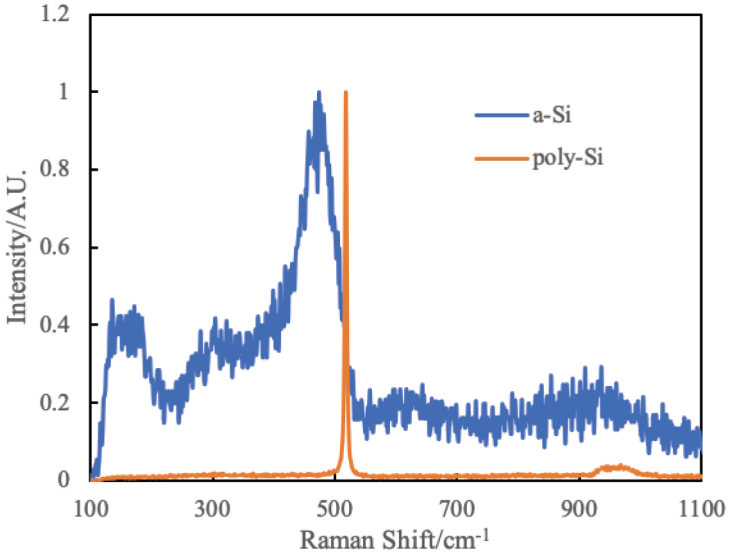

Fig. 3. Raman spectra obtained from the a-Si film (blue) and on a laser irradiated track (orange).

assigning the known FWHM value of 2.7 cm^{-1} of the Lorentzian component helped us determine the Gaussian component of the Voigt function which is associated with the response of the instrument. Applying a Voigt function fit to the Raman peaks that were obtained from the laser irradiated tracks and by taking into account the fixed Gaussian instrument response, as determined by the Voigt fit to the reference spectrum, we obtained the FWHM values for the Lorentzian component that corresponds to the laser crystallized material. The smallest FWHM value that was obtained in this manner was ~ 3 cm^{-1}, (corresponding to a laser intensity of 6 W/cm^2), which is decisively wider compared with the single crystal reference. This result indicates that the quality of laser crystallized tracks in a planar film is not expected to be as as good as in laser-induced crystallization of pre-structured a-Si ridges and capillaries [7,9].

2.3. X-Ray diffraction

Micro-focus X-Ray diffraction (XRD) was employed for the analysis of the pre-etched laser tracks. A focussed X-Ray beam with size that is comparable to the laser-crystallized tracks was used to interrogate the crystal content across and along the laser irradiated tracks. This capability was made available to us at the I18 beam line of Diamond (synchrotron) light source in Harwell campus, Oxfordshire. We used the X-Ray beam in a grazing incidence configuration, so that the beam's footprint forms an oval pattern on the sample with a long axis of ~30 μm and short axis of ~2 μm. The long axis was aligned along the length of the laser tracks allowing a quick comparison on the crystal content of the laser processed area while maximizing the overlap of the beam with the laser crystallized track, thus making full use of the beam. The spatial resolution of the measurement is compromised in the longitudinal direction but it is maintained on the transverse direction. This configuration allows for a qualitative investigation that is based on the number of a diffraction events, which appear on a sector that contains a single quadrant of the Debye cones. A more detailed description of the micro-focus XRD arrangement and mode of investigation is given in [7].

The focussed X-Ray beam was scanned in the lateral direction to reveal changes of the crystalline content across the laser tracks, where the effect of the intensity variation of the laser beam is expected to be more pronounced. A qualitative investigation based on the number of

Optical Materials EXPRESS

observed scattering events in the lateral direction showed that the number of scattering events near the edge of the tracks is significantly larger (in some cases producing continuous Debye cone arcs) as compared to the central region, indicating that the peripheral region consists of smaller crystallites. This observation reflects the variation of the temperature profile that is produced by the absorption of the laser beam with a Gaussian intensity profile. Multiple scattering events were recorded in the central sector of all tracks that were investigated, thus confirming the results obtained with Raman spectroscopy.

2.4. Selective etching

The selective etching step that reveals the poly-Si superstructures involves the use of Secco-etch, a combination of chemical agents used as a tool for the visualisation of crystalline domains in poly-Si [14]. It consists of potassium dichromate ($K_2Cr_2O_7$) and Hydrofluoric Acid (HF) diluted in DI water to control the etch rate according to the application specifics. The potassium dichromate component of the mixture oxidises weak Si-Si bonds, found in a-Si and in the Si crystal domain boundaries, producing SiO_2, which is subsequently etched by HF.

When applied to the laser-crystallized tracks, which are formed within a-Si films, Secco-etching removes the a-Si part of the film, in this way revealing only the poly-Si sections which form ridge structures. The width of the resulting ridges was compared to the width of the laser irradiated tracks as a function of: laser spot size, laser intensity and thickness of the initial a-Si film. The scanning speed was kept constant at 170 μm/s.

The etching duration was set as the time required to remove completely the a-Si planar film. The etch rate for a-Si was estimated to be ~100 nm/s for the dilution of the Secco mixture that was here.

The width of the laser tracks was measured before etching using optical microscopy and was compared to that of the resulting ridges. The lateral limits of the tracks before etching are well identifiable and therefore reliably measured as shown in Fig. 4(a). Figure 4(b) shows the same track, after Secco-etching. Initial observation of Fig. 4 indicates that i) the width of the revealed ridge appears to be very similar to the pre-etched track width and ii) the optical microscopy image of the track after etching (b) shows a qualitative difference between the central section and the periphery of the track.

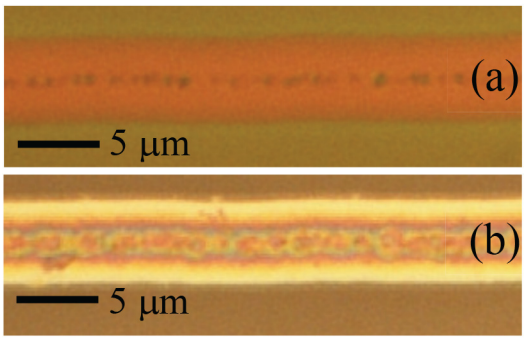

Fig. 4. Optical microscopy images of a laser irradiated track (a) before and (b) after Secco-etching. Such images were used to measure the widths of the tracks. The substrate is silica-on-silicon.

Figure 5 shows plots of the laser irradiated track widths and the resulting ridge widths as a function of laser intensity and for two different film thicknesses (210 nm and 425 nm). The main observation is that the width of the resulting ridge is very similar to the width of the visible laser track with the exception of tracks that correspond to the lower end of intensities. The ridge width appears to scale with the laser intensity (for each spot size). At low intensity levels it is only in

Optical Materials EXPRESS

the central part of the focussed laser beam where the temperature is high enough to melt the a-Si film therefore the visible laser tracks and the resulting ridges are narrower than the measured $1/e^2$ beam size. As the laser intensity increases the temperature in the peripheral sectors of the tracks increases causing the central melt zone to expand towards the periphery thus, resulting in widths which are larger than the $1/e^2$ beam size.

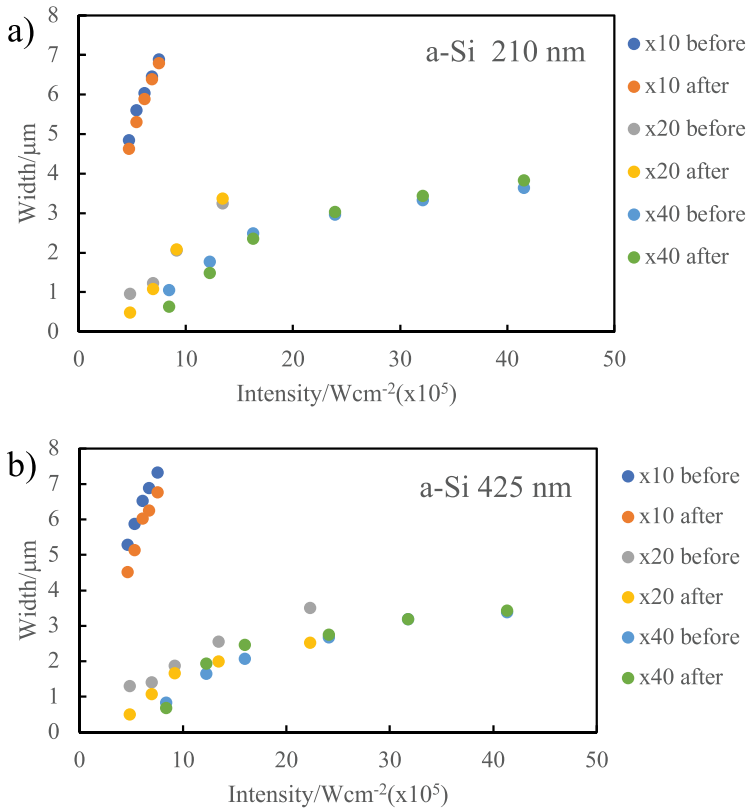

Fig. 5. Plots of the measured laser track widths before etching and ridge widths after etching as a function of laser intensity for different laser spot sizes (measured at $1/e^2$), 3 μm, 1.2 μm and 0.8 μm, (using ×10, ×20 and ×40 microscope objectives respectively). Plot (a) corresponds to initial a-Si film thicknesses of 210 nm and plot (b) to 425 nm

These results suggest that, within the range of experimental conditions used here, the most significant parameter that influences the width of the resulting ridges is the laser intensity. The thickness of the film does not appear to play an important role in the width of the laser-crystallized ridge. This indicates that the temperature distributions that are formed due to the absorption of the laser radiation is similar for these films as well. If there was any difference in the crystal domain size for the two different thicknesses they were too subtle to register in the Raman spectroscopy and X-Ray diffraction data.

Figure 6 shows SEM images of etched poly-Si ridges, which are produced on (a) silica-on silicon and (b) SiO_2 using the same irradiation conditions. In both specimens the a-Si film is grown on SiO_2. However, in the case of silica-on-silicon the SiO_2 layer is just a ~5 μ m thick layer on top of crystalline Si, which in principle, would have some implications in the heat transport properties of the substrate and consequently affect the laser-induced temperature distribution. Both SEM images show ridges of the same width that consist of a solid central section (~3 μm in width) and two peripheral sections either side that appears to be porous. The peripheral porosity

Optical Materials EXPRESS

is more pronounced in the ridge of Fig. 6(b), which correspond to the pure SiO_2 substrate. The difference in appearance however is attributed to the fact that that particular sample was slightly over etched as compared to the silica-on silicon grown sample rather than on any substantial differences in the crystallization quality. As suggested by the qualitative micro-focus XRD investigation, the central sector consist of fewer larger crystals while the periphery consists of Si crystal nano-domains. It is anticipated that in the central sector the temperature is high enough to induce complete melting of the a-Si, which is a requirement for the production of large crystal domains [8,15], while the periphery remains solid throughout the process and therefore contains crystal nano-domains only. The sharp border between the two sectors that can be observed in the SEM images of Fig. 6(a,b), marks the extent of the melt zone. Figure 6(c) shows a cross section of a ridge structure. The cross section was prepared by polishing the edge of a fully processed sample (on a SiO_2 substrate) that contained poly-Si ridges to be used for waveguide transmission experiments. The cross section shows that the peripheral sections are partially removed by the etchant, however at a lower rate compared to a-Si, forming a trapezoid cross section. For clarity the profile of the cross section is marked with a dash-line. The debris that is observed in the SEM image corresponds to wax residue from the polishing process. The shape of the poly-Si superstructures corresponds to the laser-irradiated pattern, which suggests that more complex structures can be produced by laser writing. Here we present examples of curved and joint-up structures such as a $20\mu m$ radius ring structure placed next to a straight ridge in Fig. 6(d) and a Y-junction in Fig. 6(e).

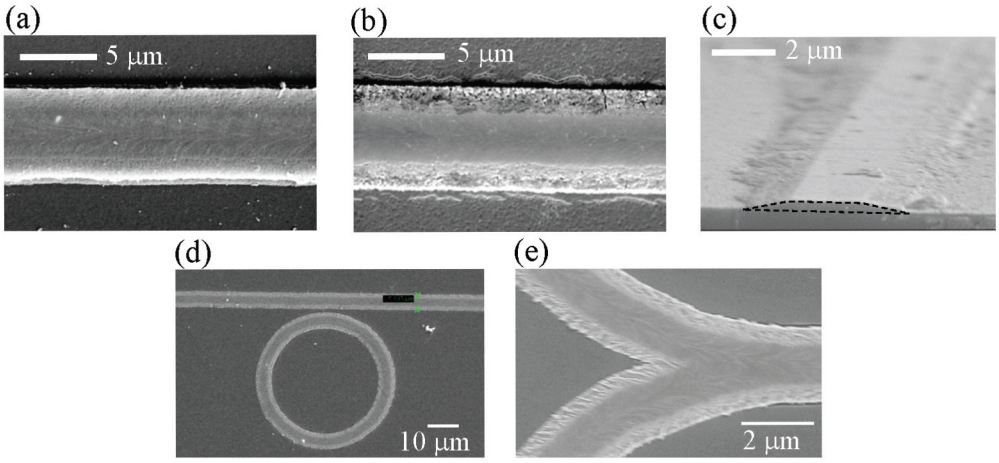

Fig. 6. SEM images of laser written poly-Si superstructures; top view SEM images of etched ridges on (a) silica-on-silicon and (b) on SiO_2 substrate. The two ridges were prepared using the same laser irradiation conditions. (c) Polished end face of a single ridge fabricated on SiO_2. The dash-line outlines the trapezoid shape of the ridge cross section. More complex poly-Si ridge structures: (d) ring ($20\mu m$ radius), next to a straight ridge, and (e) a Y-junction.

2.5. Ridge waveguides

A set of linear poly-Si ridge structures was produced on a SiO_2 substrate to investigate waveguide transmission. The height of the ridges was $\sim 400nm$ and the width $\sim 6\mu m$. The sample was edge-polished, using a standard mechanical polishing protocol, on both ends, along a plane perpendicular to the direction of the ridges to allow for "end-fire coupling" of light and for the detection of light emerging from the ridge structures. The sample was prepared using a laser spot size of 3 μm ($\times$10 objective) and a narrow range of laser intensities restricted to those that produced the best crystallization results.

Optical Materials EXPRESS

A free space optical arrangement was employed for the characterization of the waveguide transmission. This arrangement utilised a linearly polarised HeNe laser source emitting at λ=1523 nm, which was focused using a microscope objective onto one of the polished edges of the sample. A second microscope objective was used to image the output face of the sample and to collect the light that emerged from the output face of the ridge waveguide and to form an image of the near field mode shape onto an IR camera.

Only transmission of the TM modes was observed in these ridge structures. The inset of Fig. 7 shows a near field intensity profile of the propagating mode captured using an IR camera suggesting that propagation occurs in the fundamental mode, which is unexpected given the lateral dimension of the structure. The shape of the waveguide ridge could provide some explanation for this. Figure 6(c) indicates that the cross section of the ridge is trapezoidal, with the side walls sloping towards the substrate at an angle of ~75^{o} with respect to the normal, while the etch-resistive core of the ridge waveguide has a width of only ~3 μm. This sloped sidewall suggests that light propagating in the waveguide experiences a graded index in the lateral direction. Additionally, higher order modes "see" more of the sidewall roughness and therefore should experience higher propagating loss. However full analysis of the waveguide transmission is beyond the scope of this report.

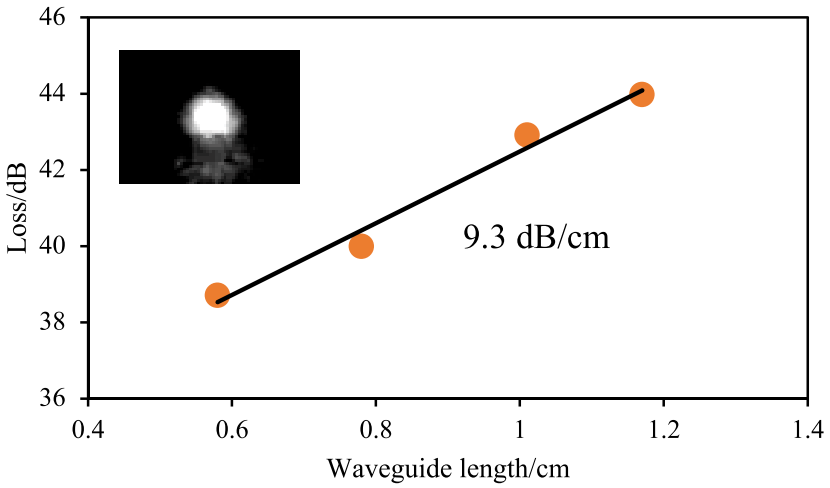

Fig. 7. Optical loss (in dB) as a function of the waveguide length. These measurements were obtained by successive polishing of the output face of the sample. The inset shows a near field image of the mode profile, captured on an IR camera.

The power transmission through the waveguides was measured by replacing the camera with a power meter head. The power transmission loss through these ridge waveguide structures was estimated by using the "cut-back" method. The output facet of the sample was polished back at specific intervals and transmission measurements were performed for each length. A plot of the raw power loss (in dB) for four waveguide lengths is shown in Fig. 7 obtained from one of the waveguides. Fitting of a straight line indicates a transmission loss of 9.34 dB/cm for this particular waveguide that was produced using a laser intensity of 6.3×10^{5} W/cm^{2} and has an overall width of ~6 μm. Waveguides fabricated with intensities within 10% variation of that laser intensity exhibited similar transmission loss figures. Significant variance of the irradiating laser intensity from that optimum value resulted in much higher transmission loss.

Optical Materials EXPRESS

3. Conclusion

We have presented a method for the production of poly-Si photonic microstructures that is based on localised laser-induced crystallization of low temperature deposited a-Si planar films combined with selective etching. This method is suitable for additive manufacturing and is compatible with CMOS processing. The crystalline contents of these superstructures have been discussed and their size has been investigated as a function of laser irradiation conditions. This method, which does not require any preparatory steps such as pre-structuring, has been utilised for the fabrication of ridge waveguides that presented transmission loss of ~9 dB/cm demonstrating the potential of this cost effective method for the production of structures with photonic functionality.

Funding

Engineering and Physical Sciences Research Council (EPSRC) (EP/M022757/1).

Acknowledgments

The authors thank Dr Ozan Aktas, Stuart MacFarquhar and Dr. K. Ignatyev along with Diamond Light Source staff for their assistance on beamline I18 (SP17304) that contributed to the results presented here.

References

1. G. T. Reed, "The optical age of silicon," Nature **427**(6975), 595–596 (2004).
2. B. Jalali and S. Fathpour, "Silicon photonics," J. Lightwave Technol. **24**(12), 4600–4615 (2006).
3. Y. H. D. Lee, M. O. Thompson, and M. Lipson, "Deposited low temperature silicon ghz modulator," Opt. Express **21**(22), 26688–26692 (2013).
4. Q. Fang, J. F. Song, S. H. Tao, M. B. Yu, G. Q. Lo, and D. L. Kwong, "Low loss (6.45db/cm) sub-micron polycrystalline silicon waveguide integrated with efficient sion waveguide coupler," Opt. Express **16**(9), 6425–6432 (2008).
5. J. S. Orcutt, S. D. Tang, S. Kramer, K. Mehta, H. Li, V. Stojanović, and R. J. Ram, "Low-loss polysilicon waveguides fabricated in an emulated high-volume electronics process," Opt. Express **20**(7), 7243–7254 (2012).
6. M. Douix, C. Baudot, D. Marris-Morini, A. Valéry, D. Fowler, P. Acosta-Alba, S. Kerdilès, C. Euvrard, R. Blanc, R. Beneyton, A. Souhaité, S. Crémer, N. Vulliet, L. Vivien, and F. Boeuf, "Low loss poly-silicon for high performance capacitive silicon modulators," Opt. Express **26**(5), 5983–5990 (2018).
7. Y. Franz, A. F. J. Runge, S. Z. Oo, G. Jimenez-Martinez, N. Healy, A. Khokhar, A. Tarazona, H. M. H. Chong, S. Mailis, and A. C. Peacock, "Laser crystallized low-loss polycrystalline silicon waveguides," Opt. Express **27**(4), 4462–4470 (2019).
8. J. Michaud, R. Rogel, T. Mohammed-Brahim, and M. Sarret, "Cw argon laser crystallization of silicon films: Structural properties," J. Non-Cryst. Solids **352**(9-20), 998–1002 (2006).
9. N. Healy, S. Mailis, N. M. Bulgakova, P. J. A. Sazio, T. D. Day, J. R. Sparks, H. Y. Cheng, J. V. Badding, and A. C. Peacock, "Extreme electronic bandgap modification in laser-crystallized silicon optical fibres," Nat. Mater. **13**(12), 1122–1127 (2014).
10. R. E. Schropp, "Present status of micro- and polycrystalline silicon solar cells made by hot-wire chemical vapor deposition," Thin Solid Films **451-452**, 455–465 (2004).
11. P. Brogueira, J. Conde, S. Arekat, and V. Chu, "Low filament temperature deposition of a-Si:H by hot-wire chemical vapor deposition," J. Appl. Phys. **78**(6), 3776–3783 (1995).
12. K.-Y. Chan, D. Knipp, A. Gordijn, and H. Stiebig, "Influence of crystalline volume fraction on the performance of high mobility microcrystalline silicon thin-film transistors," J. Non-Cryst. Solids **354**(19-25), 2505–2508 (2008).
13. J. Filik, P. May, S. Pearce, R. Wild, and K. Hallam, "XPS and laser Raman analysis of hydrogenated amorphous carbon films," Diamond Relat. Mater. **12**(3-7), 974–978 (2003).
14. A. Abbadie, S. W. Bedell, J. M. Hartmann, D. K. Sadana, F. Brunier, C. Figuet, and I. Cayrefourcq, "Study of HCl and secco defect etching for characterization of thick sSOI," J. Electrochem. Soc. **154**(8), H713–H719 (2007).
15. N. Healy, M. Fokine, Y. Franz, T. Hawkins, M. Jones, J. Ballato, A. C. Peacock, and U. J. Gibson, "Co2 laser-induced directional recrystallization to produce single crystal silicon-core optical fibers with low loss," Adv. Opt. Mater. **4**(7), 1004–1008 (2016).